Interaction of a Toxin from the Scorpion Tityus serrulatus with a Cloned K + Channel from Squid (sqKv1A) †

ARTICLE *in* BIOCHEMISTRY · JUNE 2001

Impact Factor: 3.02 · DOI: 10.1021/bi010173g · Source: PubMed

8 AUTHORS, INCLUDING:

Todd Tenenholz
Vanderbilt University
22 PUBLICATIONS **319** CITATIONS
SEE PROFILE

David Joseph Weber
University of Maryland, Baltimore
126 PUBLICATIONS **3,843** CITATIONS
SEE PROFILE

Interaction of a Toxin from the Scorpion *Tityus serrulatus* with a Cloned K^+ Channel from Squid (sqKv1A)†

K. C. Ellis,‡ T. C. Tenenholz,‡ H. Jerng,§ M. Hayhurst,§ C. S. Dudlak,§ W. F. Gilly,§ M. P. Blaustein,|| and D. J. Weber*,‡

Departments of Biochemistry and Molecular Biology and of Physiology, University of Maryland School of Medicine, Baltimore, Maryland 21201, and Hopkins Marine Station, Department of Biological Sciences, Stanford University, Pacific Grove, California 93950

Received January 26, 2001; Revised Manuscript Received March 12, 2001

ABSTRACT: A toxin from the scorpion *Tityus serrulatus* (TsTX-Kα) blocks native squid K^+ channels and their cloned counterpart, sqKv1A, at pH 8 ($^{native}K_d \approx 20$ nM; $^{sqKv1A}K_d \approx 10$ nM). In both cases, decreasing the pH below 7.0 significantly diminishes the TsTX-Kα effect (pK = 6.6). In the cloned squid channel, the pH dependence of the block is abolished by a single point mutation (H351G), and no change in toxin affinity was observed at higher pH values (pH ≥8.0). To further investigate the TsTX-Kα−sqKv1A interaction, the three-dimensional structure of TsTX-Kα was determined in solution by NMR spectroscopy, and a model of the TsTX-Kα−sqKv1A complex was generated. As found for other α-K toxins such as charybdotoxin (CTX), site-directed mutagenesis at toxin residue K27 (K27A, K27R, and K27E) significantly reduced the toxin's affinity for sqKv1A channels. This is consistent with the TsTX-Kα−sqKv1A model reported here, which has K27 of the toxin inserted into the ion conduction pathway of the K^+ channel. This toxin-channel model also illustrates a possible mechanism for the pH-dependent block whereby lysine residues from TsTX-Kα (K6 and K23) are repelled by protonated H351 on sqKv1A at low pH.

The identification and characterization of a number of small polypeptides from the venoms of scorpions, snakes, and spiders have aided the study of K^+ channels (*1*, *2*). Several members of the α-K[1] family of scorpion toxins are well characterized, and they all adopt an α/*β* scaffold structure with a single helix anchored to a two- or three-stranded antiparallel *β*-sheet by three conserved disulfide bridges (C7−C28, C13−C33, and C17−C35; Table 1) (*3*, *4*). Although the overall fold of these α-K toxins is very similar, there are subtle variations among them in amino acid sequence, the size of the *β*-sheet, the type of *β*-turn, and/or the type of helix (i.e., α-helix vs 3_{10}-helix). These differences in toxin structure affect the placement of side chain moieties; thus, the selectivity that various scorpion toxins have for the outer vestibule of different K^+ channels is typically quite distinct (*3*).

A "complementary" variability exists in several key residues on the α-subunits that form the tetrameric K^+ channels, e.g., the positions of T449 and F425 of *Shaker* B (Table 2). There is essentially no conservation at these positions, even between very closely related genes such as mammalian Kv1.1−1.6 (*5*, *6*). Single amino acid changes at some of these positions on the channel as well as complementary positions on the toxin can produce very large changes in binding affinity. The lack of conservation can make these changes in affinity difficult to predict, however. It is thus valuable to study in more detail the interactions between naturally occurring toxins and their high-affinity K^+ channel partners.

† This work was supported in part by National Institutes of Health Grants NS-17510 (to W.F.G.), NS16106 (to M.P.B.), and NS34622 (to the late M. C. Wier and M.P.B.), by National Institutes of Health Training Grant P32 GM08181 at the University of Maryland School of Medicine, and by SRIS and DRIF funding from the State of Maryland (to D.J.W.). This study made use of the NMR facility at the University of Maryland at Baltimore (UMB), which was supported by funds from the University of Maryland and the NIH shared instrumentation grant program (Grant S10RR10441 to D.J.W.).

* To whom correspondence should be addressed: Department of Biochemistry and Molecular Biology, University of Maryland School of Medicine, 108 N. Greene St., Baltimore, MD 21201. Telephone: (410) 706-4354. Fax: (410) 706-0458. E-mail: dweber@umaryland.edu.

‡ Department of Biochemistry and Molecular Biology, University of Maryland School of Medicine.

§ Stanford University.

|| Department of Physiology, University of Maryland School of Medicine.

[1] Abbreviations: AgTX2, agitoxin variant 2; CTX, charybdotoxin; DEAE, diethylaminoethyl; DEPC, diethyl pyrocarbamate; DQF-COSY, double-quantum-filtered correlation spectroscopy; DRG, dorsal root ganglion; EDTA, ethylenediamine-*N*,*N*,*N*′,*N*′-tetraacetic acid; HPLC, high-pressure liquid chromatography; IPTG, isopropyl thio-*β*-D-galactoside; LB, Luria broth; NMR, nuclear magnetic resonance; NTX, noxiustoxin; NOE, nuclear Overhauser effect; NOESY, NOE spectroscopy; OD, optical density; PMSF, phenylmethanesulfonyl fluoride; RBS, rat brain synaptosomes; rmsd, root-mean-square deviation; ROESY, rotating-frame NOE spectroscopy; SDS−PAGE, sodium dodecyl sulfate−polyacrylamide gel electrophoresis; sqKv1A, squid Kv1 potassium channel; TsTX-Kα, tityustoxin K-α; TOCSY, total correlation spectroscopy; TPPI, time-proportional phase incrementation; TSP, 3-(trimethylsilyl)[2,2,3,3-$^2H_4$]propionate. α-K toxin refers to the previously described family of potassium channel blocking peptides which are homologous to CTX.

10.1021/bi010173g CCC: $20.00
Published on Web 04/26/2001

Table 1: Sequence Alignment of Selected α-K Toxins

Toxin	Sub-Family[a]	Sequence
		1 5 10 15 20 25 30 35
CTX	1.1	Z F T N V S C T T S K E C W S V C Q R L H N T - S R G **K** C M N K K C R C Y S
NTX	2.1	T I I N V K C T S P K Q C S K P C K E L Y G S S A G A **K** C M N G K C K C Y N
TsTX-Kα	4.1	V F I N A K C R G S P E C L P K C K E A I G K - A A G **K** C M N G K C K C Y P

[a] Subfamilies have been previously described (*3*, *4*, *54*).

Table 2: Sequence Alignment of Selected Pore Regions of Cloned K^+ Channels[a]

Channel		Sequence
		Pore
sqKv1A	347	T E Q S H F K S I P D S F W W A V V T M T T V G Y G D M S P V G V
KscA	54	A P G A Q L I T Y P R A L W W S V E T A T T V G Y G D L Y P V T L
Shaker	421	S E N S F F K S I P D A F W W A V V T M T T V G Y G D M T P V G F
Kv1.3	376	D P S S G F N S I P D A F W W A V V T M T T V G Y G D M H P V T I

[a] The properties of these K^+ channels have been previously described (*3*, *30*, *55*).

One toxin from the scorpion *Tityus serrulatus*, TsTX-Kα, selectively blocks the classic "delayed rectifier" K^+ conductance (g_K) in native squid giant fiber lobe (GFL) neurons and giant axons (*7*). The channels underlying the squid g_K are proposed to be comprised of sqKv1A α-subunits (sqKv1A; see Table 2), which was cloned from a stellate ganglion cDNA library (*8*, *9*). Transcripts of sqKv1A mRNA are found only in the GFL portion of the ganglion, and sqKv1A protein is expressed in both GFL cell bodies and giant axons. Macroscopic electrophysiological properties of sqKv1A channels expressed in *Xenopus* oocytes are in general similar to those observed for the native g_K in GFL neurons, and single-channel properties are also generally consistent between the two types of channels. Taken together, these features make sqKv1A α-subunits good candidates for forming the native "20 pS" K^+ channels in GFL neurons (*10*) and in the giant axon (*11*). These 20 pS channels are thought to underlie the vast majority of macroscopic g_K in these preparations.

In this paper, we examine at the molecular level the interaction between TsTX-Kα and the native K^+ channels in squid GFL neurons and cloned sqKv1A channels expressed in *Xenopus* oocytes. These studies include (i) characterizing the pH-dependent block of sqKv1A and native channels by TsTX-Kα, (ii) determining the three-dimensional structure of TsTX-Kα by NMR spectroscopy, (iii) showing that K27 is critically important for the toxin−channel interaction as found previously for several other α-K toxin−channel interactions, and (iv) modeling the TsTX-Kα−sqKv1A interaction. This model predicts novel toxin−channel interactions, and it can explain the pH dependence observed for the block of the sqKv1A channel by the toxin. Some of the work in this paper has been presented previously in preliminary form (*12*, *13*).

MATERIALS AND METHODS

Materials. All NMR buffers were passed through Chelex-100 resin (Bio-Rad, Hercules, CA) to remove trace metals. Perdeuterated Tris, d_{11}-Tris [1 M solution in D_2O (>98.7 at. %)], was purchased from C/D/N Isotopes, Inc. (Vandreuil, PQ), and D_2O (100.0 at. %, low in paramagnetic impurities) was purchased from Aldrich Chemical Co. (Milwaukee, WI). Charybdotoxin (CTX) was a gift from T. Bengenisich (University of Rochester Medical School, Rochester, NY). All other reagents were of the highest quality commercially available.

Preparation of Recombinant TsTX-Kα. Expression and purification of milligram quantities of TsTX-Kα were performed using procedures similar to those described previously (*14*, *15*). The expression plasmid was constructed by inserting a synthetic gene encoding TsTX-Kα into the pSR9 expression plasmid and placing it under the control of a T7 promoter. In this construct, the toxin was part of a 40 kDa fusion protein containing the T7 gene 9 sequence, the pFLAG epitope, and an enterokinase cleavage site linked to the N-terminus of the toxin. Typically, *Escherichia coli* BL21(DE3) cells transformed with the expression plasmid were cultured in 8−10 L of LB at 37 °C and induced with IPTG (0.5 mM). Following lysozyme treatment [in 10 mM Tris buffer (pH 8) containing 50 mM NaCl, 2 mM EDTA, 2 mg/mL lysozyme, 0.14 mg/mL PMSF, 0.2 μg/mL leupeptin, 0.2 μg/mL pepstatin, and 0.04% β-mercaptoethanol] and sonication, the soluble fusion protein represented the major band in an SDS−PAGE gel of the cell lysates. At 4 °C, DNA was removed by centrifugation after the slow addition of streptomycin sulfate to a final concentration of 3%. The fusion protein was then precipitated by the slow addition of solid ammonium sulfate at 4 °C to a final concentration of 50%, dialyzed into low salt, and separated from other proteins using DEAE anion exchange chromatography with a linear salt gradient of 50 to 500 mM NaCl. Dialysis of the fusion protein into a low-salt buffer [10 mM Tris and 1 mM β-mercaptoethanol (pH 7.0)] preceded treatment (24 h at 37 °C) with fresh enterokinase (200 units of enzyme/mg of fusion protein; Invitrogen, Carlsbad, CA) in 5 mM $CaCl_2$. HPLC separation on an Aquapore CX-300 cation exchange column (Pierce, Rockford, IL), followed by reverse phase chromatography on an Aquapore RP-300/C18 column (Pierce), yielded pure TsTX-Kα (>99%). HPLC solvents and trace amounts of metals were removed prior to NMR spectroscopy using two rounds of dialysis in 500 Da molecular mass cutoff membranes (Spectrapor, Los Angeles, CA) with deuterated Tris [0.25 mM d_{11}-Tris (pH 7.4)] and 0.03% Chelex-100 (Bio-Rad) in the dialysate buffer. Electrospray mass spectroscopy showed that the expressed toxin samples consisted of a single component (>99%) of the correct molecular mass,

and their protein sequences were confirmed using standard methods.

TsTX-Kα is also commercially available as both a recombinant toxin (Sigma-Aldrich, St. Louis, MO) and a synthetic toxin (Peptides International, Louisville, KY, and several other companies). In experiments with synthetic TsTX-Kα, the toxin was found to block both the rapidly inactivating and noninactivating components in a screen with the rat brain synaptosome flux assay (data not shown), whereas native (and recombinant) TsTX-Kα blocks only the noninactivating component (*16*). Additionally, a one-dimensional NMR spectrum of the synthetic toxin revealed an extraneous peak that is not seen in the spectrum of the recombinant toxin. Following extensive dialysis (1000 Da molecular mass cutoff) and lyophilization, however, the synthetic toxin displayed the same specificity in the synaptosome assay (*17*) as did native TsTX-Kα. The extraneous resonance observed in the one-dimensional NMR spectrum also disappeared after the additional purification of synthetic TsTX-Kα (data not shown). In contrast to the synthetic toxin, the recombinant toxin was indistinguishable from the native toxin in its ability to block K^+ channels in RBS (*16*). Therefore, for these studies, the recombinant toxin prepared in our laboratory was used exclusively.

Site-Directed Mutagenesis of TsTX-Kα. Toxin mutagenesis was performed using the QuikChange site-directed mutagenesis kit (Stratagene, La Jolla, CA). The pSR9 plasmid (*18*) containing the gene for the wild-type toxin purified from *E. coli* was used as a template. Two complementary oligonucleotide primers containing the desired mutation were synthesized. During thermocycling, the primers were annealed to the template and extended with *Pfu*Turbo DNA polymerase to incorporate the mutation into double-stranded, nicked DNA. Following removal of the template DNA by treatment with *Dpn*I, mutated plasmids were transformed into XL-1 Blue *E. coli* (Stratagene) for propagation and to repair DNA nicks. Transformed cells were screened for mutant plasmids, and successfully mutated plasmids were purified from the XL-1 Blue cells and transferred into BL21(DE3) cells for expression and purification of the mutant TsTX-Kα. Sequences of the mutated plasmids were confirmed by DNA sequencing. The mutant TsTX-Kα polypeptides were prepared using the same methods described above for the wild-type recombinant toxin.

Electrophysiology with Xenopus Oocytes. Stage IV oocytes from adult *Xenopus laevis* (NASCO, Fort Atkinson, WI) were isolated, treated with collagenase, and cultured following standard procedures described in detail elsewhere (*19*). Full-length cRNAs encoding wild-type (wt) and mutant sqKv1A α-subunits (see below) were transcribed from a pBSTA-based expression vector (*9*) using T7 polymerase (Message Machine, Ambion, Austin, TX) after linearizing with *Not*I. Mutants of sqKv1A-pBSTA were created with specific oligonucleotide primers and the QuikChange site-directed mutagenesis kit as described above for toxin mutagenesis. All mutations were confirmed by sequencing. Most experiments with sqKv1A in this study used the T1 domain mutant (G87R) and/or an N-terminal deletion mutant, ΔV5. These mutations lead to elevated expression levels with no changes in other functional properties when compared to wild-type sqKv1A (*19*).

Oocytes were injected with 0.25−5 ng of capped cRNA, depending on the desired expression level for the particular α-subunit employed, and were then maintained at 17−18 °C in ND96 [96 mM NaCl, 2 mM KCl, 1.8 mM $CaCl_2$, 1 mM $MgCl_2$, 2.5 mM sodium pyruvate, and 5 mM HEPES (pH 7.2)] supplemented with 2.5 mM sodium pyruvate and 50 μg/mL gentamycin for 24−48 h until recordings were carried out.

Two-microelectrode voltage-clamp experiments were carried out at room temperature (22−25 °C) in low-Cl ND96 (96 mM sodium gluconate, 2 mM potassium gluconate, 2 mM $CaCl_2$, and 2 mM $MgSO_4$) along with the appropriate pH buffer (5−10 mM), i.e., MES (pH 5−6), HEPES (pH 6.5−8), or CAPSO (pH 8−9). K^+ currents (I_K) from wild-type and mutant sqKv1A channels tend to "run down" in normal ND96, and replacement of Cl with gluconate greatly increased the stability of I_K. The basis for this effect has not been investigated in detail. Substitution of Cl with gluconate did not alter the apparent K_d of wild-type sqKv1A channels for TsTX-Kα (data not shown).

For recordings, we employed a conventional amplifier (OC-725B from Warner Instruments, Hamden, CT, or GeneClamp from Axon Instruments, Foster City, CA). Microelectrodes were filled with 3 M KCl and had resistances of <1 MΩ. Data acquisition, pulse generation, and on-line signal processing (P/-4 treatment to remove linear ionic and capacity currents) were carried out using a personal computer-based system designed by D. R. Matteson (University of Maryland School of Medicine). The holding potential was −70 or −60 mV. The effect of toxins was typically assayed using brief (10−15 ms) steps to 0 mV. This procedure was found to minimize voltage-dependent effects and dissociation of toxin, which can occur with long pulses, particularly with some sqKv1A mutants (unpublished data).

Electrophysiology on Squid GFL Neurons. Conventional whole-cell recordings from dissociated GFL neurons were carried out as previously described (*7*). The external solution contained 470 mM NaCl, 10 mM KCl, 10 mM $CaCl_2$, 20 mM $MgCl_2$, 20 mM $MgSO_4$, and 0.2 mM tetrodotoxin with pH buffering as described above. The internal solution contained 20 mM KCl, 80 mM potassium glutamate, 50 mM KF, 10 mM lysine (titrated to pH 7 with HEPES), 1 mM EGTA, 1 mM EDTA, 381 mM glycine, 291 mM sucrose, and 4 mM MgATP. The final pH was adjusted to 7.8 with tetramethylammonium hydroxide. Recordings were carried out at 14−22 °C, and properties described in this paper are not significantly temperature-sensitive over this range. The holding potential was −80 mV. I_K and the effects of toxin were assayed as described above, although most measurements were carried out at 40 mV to minimize the contribution of small inward Ca^{2+} currents present in GFL neurons (*20*). Voltage-dependent dissociation of the toxin from native channels in GFL neurons appears to be less pronounced than with sqKv1A expressed in oocytes (unpublished data).

Chemical Modification of Wild-Type and Mutant sqKv1A Channels. Oocytes were treated with 1 mM diethyl pyrocarbamate (DEPC; pH 7.4), a reagent selective for histidine residues on proteins. DEPC treatment in ND96 at pH 7.4 caused a progressive, irreversible decrease in the amplitude

of I_K and slowing of activation kinetics (*21*) of both wild-type and mutant channels (data not illustrated). Treatment was halted after I_K was reduced by approximately 50% (10−20 min), and the sensitivity to 100 nM TsTX-Kα (pH 7.4) was then tested.

NMR Experiments. The sample of wild-type TsTX-Kα used for the NMR experiments was prepared by dissolving 4.5 mg of the lyophilized recombinant toxin in a buffer containing 2.2 mM d_{11}-Tris, 0.35 mM NaN_3, 0.1 mM EDTA, and 10% D_2O to a final volume of 250 μL and a final toxin concentration of 4.53 mM. Minute amounts of cold NaOH (0.5 M) and HCl (0.5 M) were added to adjust the pH to 3.50.

Proton NMR data used in the structure calculations were collected at 600.13 MHz using a Bruker DMX-600 spectrometer (Bruker Inc., Billerica, MA) with a sweep width in both proton dimensions of 7184 Hz. In typical experiments, 2048 t_2 and 1024 t_1 data points were acquired using a relaxation delay of 1 s. Solvent suppression was achieved using the WATERGATE sequence (*22*), or by selective saturation of the H_2O and HDO resonances during the initial delay. All experiments were conducted at both 37 and 17 °C, with additional two-dimensional DQF-COSY and one-dimensional experiments performed at 32, 27, and 22 °C. Spectra were referenced to the residual water signal at the appropriate temperature value as a secondary reference to TSP [3-(trimethylsilyl)[2,2,3,3-$^2H_4$]propionate]. Data were processed off-line using FELIX (Molecular Simulations, San Diego, CA) or NMRPipe (*23*) on a Silicon Graphics Indy workstation (Silicon Graphics Inc., Mountain View, CA). Data were multiplied by a sine-squared bell and zero-filled to 2048 points in both dimensions prior to Fourier transformation.

Spin system identification and sequence specific assignments were determined using standard methods (*24*). Experiments included two-dimensional DQF-COSY, two-dimensional TOCSY data collected with a 75 ms spin-lock mixing time (*25*), and two-dimensional NOESY (*26*) experiments collected with 50, 150, and 200 ms mixing times. Additionally, a ROESY spectrum (*27*) was collected with both 75 and 150 ms spin-lock mixing times, and the resulting data were used to correct NOESY data for spin-diffusion effects. An E-COSY spectrum was recorded in D_2O to obtain passive and active $^3J_{H\alpha-H\beta}$ coupling constants (*28*).

Hydrogen exchange rates were observed by lyophilizing TsTX-Kα from H_2O and redissolving it in 99.96% D_2O at 37 °C. During the first 30 min of exchange, a series of one-dimensional experiments were carried out every 2 min to observe the most rapidly exchanging protons. For the next 30 min, one-dimensional experiments were carried out every 5 min. Additional one-dimensional spectra were recorded 2, 3, 5, 9, 12, 24, and 49 h following the initial addition of D_2O. Two-dimensional TOCSY spectra were initiated 30 min, 180 min, 7 h, and 24 h after the addition of D_2O.

Structure Calculations. Analyses of NOESY and ROESY spectra were used to assign 569 $^1H-^1H$ NOE correlations, which were divided into strong (1.8−2.8 Å), medium (1.8−3.3 Å), weak (1.8−5.0 Å), and very weak (1.8−6.0 Å) categories. Internal calibration of cross-peak intensities was achieved by comparing several $d_{\alpha N}(i,i+3)$ correlations observed for TsTX-Kα, which have a known distance of ≈3.4 Å in α-helices, to other correlations in the same NOESY or ROESY spectrum. Rotational conformations about χ_1 were determined using a combination of $^3J_{H\alpha-H\beta}$ coupling constants and NOE intraresidue correlations ($d_{\alpha\beta}$ and $d_{N\beta}$) (*24*) and were assigned to one of three possible rotamers (χ_1 = 60°, 180°, or −60°) with a tolerance of ±40°. These χ_1 angle restraints resulted in stereospecific assignment of 13 methylene protons. $^3J_{HN-H\alpha}$ coupling constants were directly measured from the splitting of amide proton peaks with sufficient dispersion in the one-dimensional spectrum, resulting in 16 ϕ angle constraints. Amide protons with $^3J_{HN-H\alpha}$ values of <5.75 Hz were assigned a ϕ value of $-60 \pm 40°$, and protons with $^3J_{HN-H\alpha}$ values of >7.5 Hz were assigned a ϕ value of $-120 \pm 30°$. Twenty-six hydrogen bond constraints were derived from amide exchange data and NOE cross-peaks characteristic of α-helix and β-sheet secondary structural elements. These H_N-O distances were assigned a lower limit of 1.5 Å and an upper limit of 2.3 Å. The three disulfide bridges were replaced with distance constraints (2.01−2.03 Å) between the S_γ atoms during the matrix subembedding step. In support of these H-bonds and disulfide bond pairings, structures calculated without these hydrogen and disulfide bond constraints showed no significant changes (backbone rmsd for average structures of <0.65 Å).

Structural calculations were performed using the program X-PLOR (*29*) as described previously for other α-K toxins (*14*, *15*). Initial structures were calculated with only the unambiguously assigned NOE correlations. These structures were used to resolve ambiguities in the spectra and assign additional NOE correlations. A total of 342 inter-residue, 201 intraresidue, and 26 hydrogen bonding distance constraints, as well as 13 dihedral angle (χ_1) and 16 backbone angle (ϕ) constraints, were used to calculate structures for TsTX-Kα (Table 3). A large number of structures (>50%)

Table 3: NMR-Derived Restraints and Statistics of NMR Structures[a]

	⟨30⟩	best
rmsds		
all constraints (569)	0.005 ± 0.001	0.004
intraresidue NOEs (201)	0.002 ± 0.001	0.003
sequential NOEs (145)	0.006 ± 0.004	0.003
medium-range NOEs (73)	0.001 ± 0.002	0.001
long-range NOEs (124)	0.005 ± 0.002	0.005
hydrogen bonds (26)	0.012 ± 0.004	0.011
dihedral constraints	0.162 ± 0.165	0.126
rmsds (covalent geometry)		
bonds (Å)	0.002 ± 0.000	0.002
angles (deg)	0.571 ± 0.006	0.577
impropers (deg)	0.383 ± 0.006	0.380
Lennard-Jones energy	−55.688 ± 8.871	−65.335
rmsds for ⟨30⟩ structures (Å)	**relative to mean**	**pairwise**
backbone (residues 2−36)	0.525 ± 0.10	0.757 ± 0.15
heavy atoms (residues 2−36)	1.052 ± 0.10	1.533 ± 0.19
backbone (all residues)	0.595 ± 0.11	0.860 ± 0.16
heavy atoms (all residues)	1.096 ± 0.10	1.601 ± 0.19

[a] "⟨30⟩" indicates the ensemble of 30 low-energy structures meeting the criteria described in Materials and Methods, and "best" indicates the lowest-energy member of the ensemble. For the ensemble of 30 low-energy structures, values are given as means ± standard deviation. The Lennard-Jones van der Waals energy was calculated using the CHARMM19 parameters and was not employed in any stage of the structure determination.

were consistent with all of the NMR-derived constraints; of these, a family of the 30 lowest-energy structures was used for the statistical analysis. None of these structures has NOE distance restraint violations of >0.20 Å or angular violations of >5° (Table 3).

Homology Model of TsTX-Kα Docked to sqKv1A. A homology model of sqKv1A was made on the basis of the crystal structure of the KscA K^+ channel (*30*). Nine residues in the turret region were changed to match the sequence of sqKv1A (A54T, P55E, G56Q, A57S, Q58H, L59F, I60K, R64D, and Y82S, corresponding to T347, E348, Q349, S350, H351, F352, K353, D357, and S375 of sqKv1A; see Table 2). The structure that had the lowest rmsd from the average structure of TsTX-Kα (from the family of 30) was manually docked into the channel based on two well-characterized toxin−channel interactions (toxin−channel, K27−Y371 and M29−S375) (*31*, *32*). Mutagenesis of the TsTX-Kα presented here indicates that K27 blocks the pore of the channel as found for other α-K toxins. Additionally, since no effect on the pH-dependent block was observed for the R8A mutation of TsTX-Kα (data not shown), the side chain of R8 is kept more than 3 Å from H351 on the channel. Energy minimization of the hand-docked model was accomplished with the computer program CHARMm (Harvard University, Cambridge, MA) using 400 steps of an adopted basis Newton−Raphson method (ABNR) (*33*) while keeping all of the above criteria satisfied.

RESULTS

TsTX-Kα Blocking of Native and Cloned Squid K^+ Channels. TsTX-Kα (100 nM, pH 9) blocks native delayed rectifier K^+ channels in squid GFL neurons (Figure 1A,i) and cloned sqKv1A channels in *Xenopus* oocytes (Figure 1A,ii) to a similar degree. Dose−response data for sqKv1A (Figure 1B) indicate an IC_{50} of ∼10 nM. As demonstrated in the lower panels of parts A,i and A,ii of Figure 1, sensitivity of both types of channels is pH-dependent with an apparent pK_a of 6−7 (Figure 1C).

Histidine residues are the most likely candidates for conferring pH sensitivity in this range, and the only histidine on the putative external surface of sqKv1A is His-351, which is located on the turret surrounding the pore at the position analogous to Phe-425 of *Shaker* B (Table 2). Additionally, there are no histidine residues in TsTX-Kα. Chemical modification of sqKv1A with a histidine selective reagent, DEPC (see Materials and Methods), substantially reduced the extent of blocking of wild-type (wt) channels by 100 nM TsTX-Kα [48 ± 5.3% (mean ± standard error of the mean, $n = 6$) vs control value of 86 ± 8.0% ($n = 3$)]. DEPC did not alter the toxin sensitivity of a mutant channel (H351G) in which His-351 was replaced with Gly [91% ($n = 2$) vs 91 ± 5.1% ($n = 3$) for wt channels]. Although the H351G mutation does not greatly alter sensitivity to TsTX-Kα (Figure 1A,iii), it abolishes pH dependence [Figure 1C (△)]. These data indicate that H351 of sqKv1A is the residue responsible for the pH dependence observed for blocking by TsTX-Kα.

Site-Directed Mutagenesis of TsTX-Kα. Mutagenesis studies of α-K toxins such as CTX indicate that K27 is the most critical residue for blocking K^+ channels such as *Shaker* (*3*, *4*, *34*−*37*). This residue protrudes off the face of the β-sheet and physically occludes the pore of the K^+ channel. To determine whether K27 is similarly responsible for TsTX-Kα blocking of sqKv1A, it was mutated (K27A, K27E, and K27R) and tested for K^+ channel block. In all three mutants, the affinity of TsTX-Kα for sqKv1A channels was reduced significantly. Conservative replacement of lysine with arginine reduced the affinity for the sqKv1A channels by ∼25-fold, and alanine or glutamate substitutions led to an increase in IC_{50} of >1000-fold (Table 4). These data indicate that K27 is critical for the TsTX-Kα block of sqKv1A as previously found for other α-K toxins.

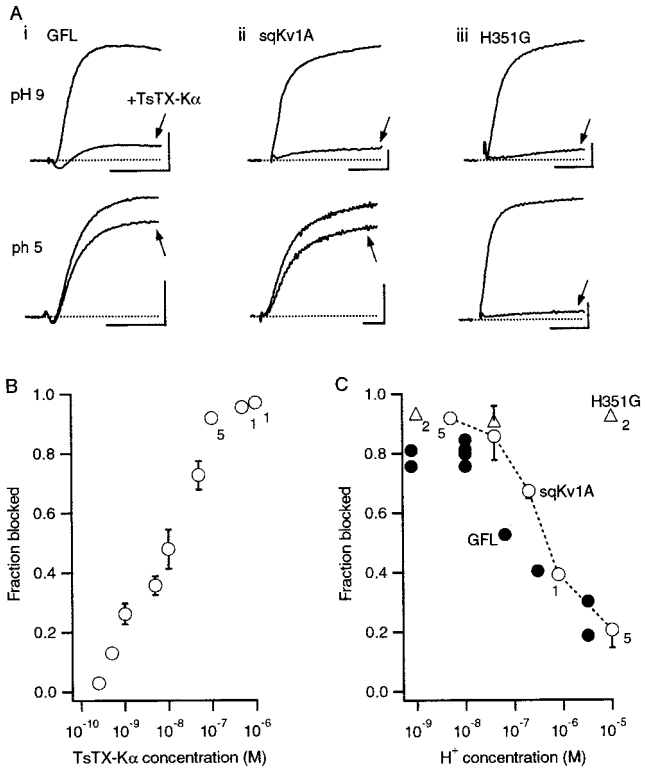

FIGURE 1: Blocking of native and cloned (sqKv1A) squid K^+ channels by TsTX-Kα. (A) Examples of I_K are illustrated at pH 9 (upper row) and 5 (lower row) before and after application of 100 nM TsTX-Kα (arrows) to GFL neurons (A,i, 40 mV) and to *Xenopus* oocytes expressing wild-type sqKv1A channels (A,ii, 0 mV) or sqKv1A channels with the H351G point mutation (A,iii, 0 mV). This mutation abolishes the pH dependence of blocking by TsTX-Kα. Vertical scale bars for GFL neurons (A,i) are 5 nA, and vetical scale bars for oocytes (A,ii and A,iii) are 1 mA. All horizontal scale bars are 5 ms. (B) Dose−response relation for wild-type sqKv1A channels expressed in *Xenopus* oocytes. Each point represents the mean ± standard error of the mean ($n = 3$), except in the cases where n is individually noted. (C) pH dependence of blocking by 100 nM TsTX-Kα is very similar for both wt sqKv1A channels in oocytes (○) and native channels in giant fiber lobe (GFL) neurons (●). SqKv1A data are means ± standard error of the mean ($n = 3$) unless otherwise indicated; for GFL neurons, the points are from individual cells. Values for H351G mutant channels are also plotted [(△) means ± standard error of the mean ($n = 3$) unless otherwise indicated].

Three-Dimensional Structure of TsTX-Kα. To model the TsTX-Kα−sqKv1A interaction, it is first necessary to determine the three-dimensional structure of TsTX-Kα by NMR spectroscopy. To complete this goal, all of the proton resonances of TsTX-Kα were assigned using standard protocols (*24*). Spin systems for all but the amino-terminal amide proton (Val-1) were identified using DQF-COSY and relayed TOCSY connectivities in H_2O. Sequence specific

Table 4: IC_{50} Values for Selected Toxins and Channels

toxin	subfamily	native squid channel IC_{50} (nM)	cloned sqKv1A channel IC_{50} (nM)
CTX	1.1	ND[a]	<30
NTX	2.1	300[b]	ND
TsTX-Kα[c]	4.1	~20 (pH 8)	10 (pH 8)
R8A[d]	–	~15	10−15
K27R[e]	–	–	~250
K27A[e]	–	–	>10000
K27E[e]	–	–	>10000

[a] ND, not determined. [b] Data published on giant axon (*45*). [c] The pH is indicated; IC_{50} is pH-dependent in squid channels (see Figure 1). The value for sqKv1A was determined by a Hill plot analysis of the data depicted in Figure 1B. The value for native squid channels was estimated from six measurements on GFL neurons at 100 nM, assuming the same concentration dependence as determined for sqKv1A (fitted Hill plot slope of 0.8). [d] The value for sqKv1A was determined from measurements at 100 ($n = 2$) and 250 nM ($n = 3$), assuming the same concentration dependence as determined for the wt toxin. The value for the native squid channel was estimated in the same manner from one measurement on a GFL neuron at 750 nM toxin. [e] Values for mutant toxins were estimated from three measurements at 100 nM (K27R) and one (K27E) or two (K27A) measurements at 100 nM, assuming the same concentration dependence as determined for the wild-type toxin.

assignments of TsTX-Kα were then made using inter-residue connectivities (αN, NN, βN, etc.) determined from the two-dimensional NOESY experiment (Table 1S of the Supporting Information). Gaps in the $d_{\alpha N}(i,i+1)$ connectivities at positions 11, 15, and 37 were expected due to the presence of proline residues, but sequential connectivities [$d_{\alpha\delta}(i,i+1)$] confirmed the location of these proline residues. Furthermore, strong $d_{\delta\alpha}(i,i-1)$ or $d_{\delta N}(i,i-1)$ NOE cross-peaks were observed between residues 11 and 10, residues 15 and 14, and residues 37 and 36. This established that all proline residues in TsTX-Kα are in the trans conformation. When these data were analyzed, all of the observable correlations were assigned in the NMR spectra such that the backbone and side chain protons of TsTX-Kα were essentially complete (>98%, BioMagResBank entry 4924).

Elements of secondary structure in TsTX-Kα were identified using NOE correlations and chemical shift values as previously described (*14*, *15*, *24*) (Figure 2). Strong $d_{\alpha N}$ connectivities from residues 2 and 3, 26−28, and 33−35 together with a positive chemical shift index (*38*) for the α-protons in these segments indicate β-strand conformation. Furthermore, 10 long-range ($i-j$) NOE interactions [$d_{\alpha N}$ (K34−I3, A26−F36, C28−K34, C35−K27, and C33−M29); d_{NN} (K27−K34 and M29−K32); $d_{\alpha\alpha}$ (F2−K34, G26−C35, and C28−C33)] establish that these three β-strands align to form a small antiparallel β-sheet (Figure 2, and Figure 1S of the Supporting Information). Two of the β-strands (G26−C28 and C33−Y36) are separated by residues 29−32 which have $d_{\alpha N}$ and d_{NN} NOE correlations expected of a tight turn (*24*). A strong d_{NN} NOE correlation, typical of a type I or I′ turn, was detected between residues 30 and 31. While a $d_{\alpha N}$ correlation was also present between these residues, its intensity was dramatically decreased in the ROESY spectrum, indicating that spin diffusion was the major contributor to this cross-peak (data not shown). While it is hard to distinguish between type I and I′ turns on the basis of NOEs alone, $^3J_{HN-H\alpha}$ coupling constants of residues 30 and 31

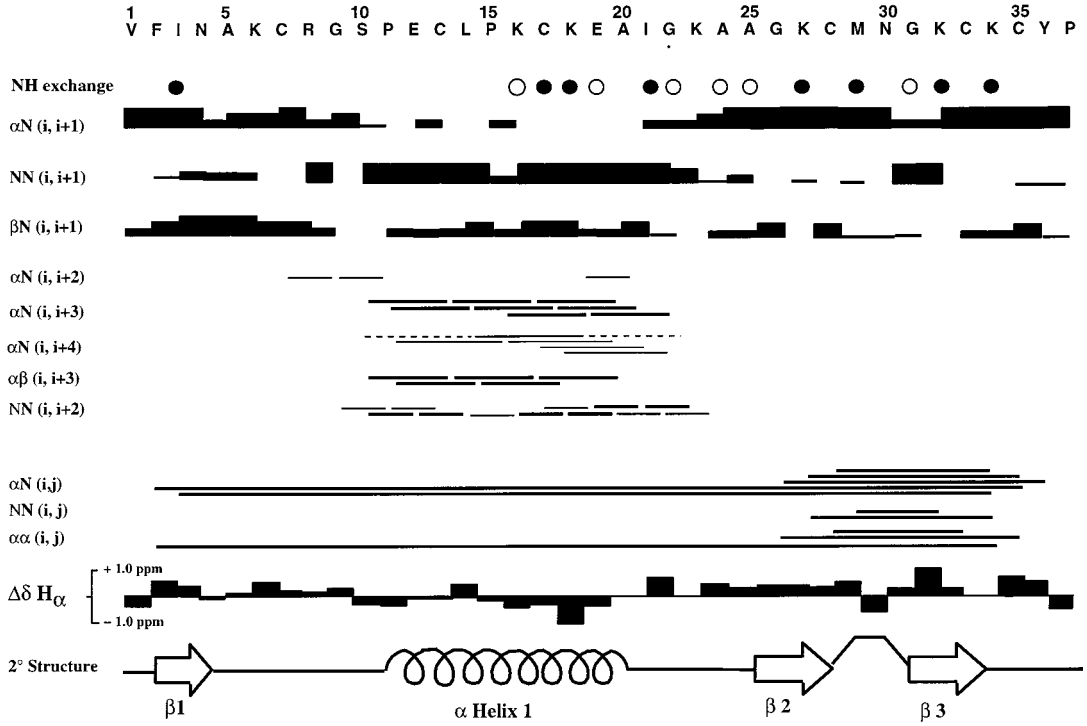

FIGURE 2: Secondary structure and NOE summary. Amino acid sequence of TsTX-Kα and summary of NOE connectivities used for sequential assignment and secondary structure determination. Data are summarized from NOESY and ROESY spectra collected at 37 °C and pH 3.50 in a 90% H_2O/10% D_2O mixture, using a NOESY mixing time of 200 ms. Overlapping NOE correlations are illustrated with dashed lines and rectangles. Very slowly exchanging amide protons are represented by black circles and slowly exchanging protons by white circles. For proline residues, sequential NOE correlations involving H_δ rather than H_N are shown. The chemical shift index for each α-proton ($\Delta\delta$ H_α) is indicated by an upward or downward pointing rectangle. The size of the rectangle represents the magnitude of the deviation from the random coil value, and no rectangle indicates a shift index of zero. Secondary structure elements determined from all of the data are also shown.

(positions 2 and 3 of the β-turn, respectively) are consistent with a type I′ β-turn (*24*).

A helical conformation was identified from residue 11 to 21 based on strong d_{NN} NOE correlations (except at Pro-11 and Pro-15; see Figure 2S of the Supporting Information) and the upfield shift in the chemical shift values for most of the α-protons of these residues with respect to random coil values (*38*). The presence of a helix from residue 11 to 21 is confirmed by the observation of eight $d_{\alpha N}(i,i+3)$ connectivities, two of which (C13−K16 and L14−C17) span the potentially helix-breaking Pro-15 residue. Six $d_{\alpha N}(i,i+4)$ NOE correlations (S10−L14, P11−P15, L14−K18, P15−E19, K16−A20, and C17−I21) and five $d_{\alpha\beta}(i,i+3)$ correlations (S10−C13, P11−L14, C13−K16, L14−C17, and K16−E19) further distinguish residues 11−21 as α-helical (Figure 2) (*24*). The presence of reciprocal side chain to backbone NOE correlations (ϵNH of Q12 to NH of E10 and βH of E10 to NH of Q12) indicates that there is an N-cap at Ser-10, and Pro-11 is the first residue of the α-helix (*39*). The slow exchange rate for the amide proton of Tyr-23, the presence of an NOE correlation between this proton and the βH of Lys-18, and a very weak NOE correlation between the αH of Lys-19 and the NH of Gly-22 are all suggestive of a C-terminal cap at Gly-22 (*39*). These results, combined with the $d_{\alpha N}(i,i+3)$ and $d_{\alpha N}(i,i+4)$ interactions involving the amide proton of Thr-21, are evidence that this residue is the last residue of the helix.

The three-dimensional structure of TsTX-Kα was calculated using 569 NOE distance constraints (∼15 per residue; Figure 3S of the Supporting Information), 13 χ_1 dihedral angle restraints, and 16 ϕ angle constraints (Table 3, and Figure 3S of the Supporting Information). The 30 accepted structures for TsTX-Kα shown in Figure 3A reveal that all of the calculated structures have the same overall backbone fold. TsTX-Kα adopts the α/β-fold which consists of a three-stranded β-sheet anchored to a single α-helix by three disulfide bonds (C7−C28, C13−C33, and C17−C35) as found for other α-K toxins. The average pairwise rmsd for these structures is 0.86 Å for backbone atoms and 1.60 Å for all heavy atoms; if the N- and C-terminal residues are excluded from the calculation, the rmsd values are 0.76 and 1.53 Å, respectively (Table 3).

When an average structure was calculated from the 30 selected structures (Figure 3B), the rmsd from this mean structure was found to be 0.60 Å for the backbone atoms and 1.10 Å for all heavy atoms (Table 2). Calculations of the structure without disulfide bonds or hydrogen bond constraints did not affect the tertiary structure. This indicates that the pairing of cysteine residues to form disulfide bonds is correct and that the hydrogen bonds included in the calculations did not significantly alter the tertiary structure (rmsd between the backbone atoms of the average structure calculated with and without these constraints was <0.65 Å). The Ramachandran diagram of the best-fit structure shows that all residues of this toxin are either in the most favored region or in the additionally allowed regions (Figure 4S of the Supporting Information). The atomic coordinates of the 30 acceptable structures and the NMR-derived restraints used to generate them have been deposited with the Protein Data Bank (Research Collaboratory for Structural Bioinformatics, New Brunswick, NJ), as entry 1HP2.

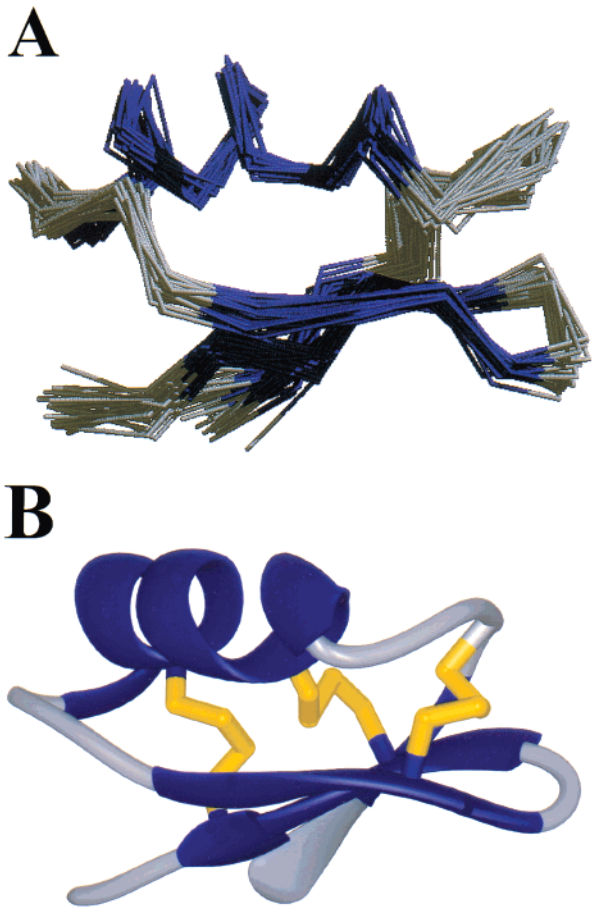

FIGURE 3: Three-dimensional structure of TsTX-Kα. (A) Overlay of α-carbons for the 30 lowest-energy NMR structures. The backbone rmsd for these 30 structures is 1.03 Å. Regions of secondary structure are shown in blue. (B) Ribbon diagram of the average structure showing its three-stranded β-sheet and α-helix with secondary structure shown in blue.

Comparison of TsTX-Kα to Other α-K Toxin Structures. The overall structure of TsTX-Kα is very similar to that of other α-K toxins, including CTX and NTX, which also adopt the same α/β-scaffold with the same disulfide bond pairings. All three of these toxins have a three-stranded antiparallel β-sheet with an α-helix separating β-strands 1 and 2. As illustrated in Figure 4A, the sequences of CTX and TsTX-Kα have differences in four residues known to be important in binding *Shaker* (Table 1 and Figure 4A). At three of these positions, CTX has large, basic moieties (K11, R25, and K31) while TsTX-Kα instead has smaller, uncharged residues (P11, A25, and G31) (refs *32* and *40*−*42* and Figure 4A). At the fourth position, TsTX-Kα has a large positively charged arginine residue (R8) while CTX has a threonine residue at this position (T8). This threonine residue on CTX interacts with F425 on the *Shaker* channel (*43*). In addition, a structural difference exists between TsTX-Kα and CTX in the β-turn connecting β-strands 2 and 3 of their β-sheet. TsTX-Kα has a type I′ turn, while CTX adopts a type I turn (*44*). This variance in turn structure results in the placement of residue 31 in different positions in TsTX-Kα and CTX (Figure 4A). Despite these differences, however, both CTX and TsTX-Kα block sqKv1A channels expressed in *Xenopus* oocytes with similar potency (TsTX-Kα, IC_{50} = 10 nM; CTX, IC_{50} < 30 nM; W. F. Gilly, unpublished).

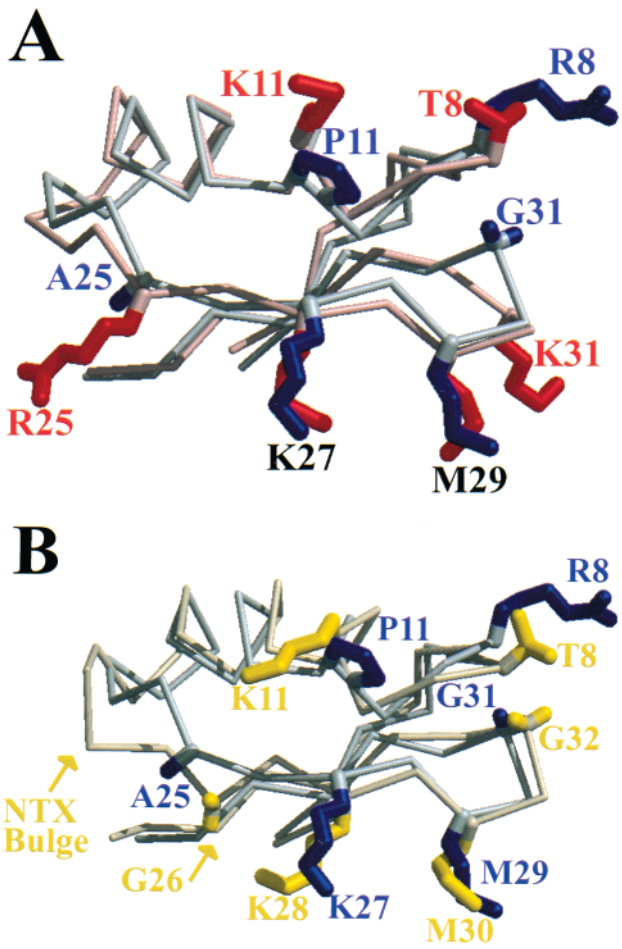

FIGURE 4: Comparison of CTX and NTX with TsTX-Kα (light red for CTX, light yellow for NTX, and light blue for TsTX-Kα). (A) Comparison of TsTX-Kα and CTX. (B) Comparison of TsTX-Kα and NTX. In both panels, selected side chain residues are shown (red for CTX, yellow for NTX, and blue for TsTX-Kα). Residues conserved between the toxins are labeled in black. Differences between the toxins (positions 8, 11, 25, and 31) are labeled in blue for CTX, yellow for NTX, and red for TsTX-Kα.

Another toxin that blocks voltage-gated squid channels with a relatively high affinity (IC_{50} = 300 nM) is noxiustoxin (NTX) (*45*). NTX and TsTX-Kα have a very similar backbone structure, including a type I′ β-turn which places G31 of TsTX-Kα and G32 of NTX in very similar positions (see Figure 4B). Additionally, like TsTX-Kα, NTX also has small, hydrophobic side chains (G26 and G32) at positions analogous to R25 and K31 in CTX. However, like CTX at positions 8 and 11, NTX has threonine and lysine residues, respectively, versus R8 and P11 as found in TsTX-Kα (Table 1).

When the sequences of TsTX-Kα and NTX are compared, one of the obvious differences is the presence of an additional amino acid (S24) in NTX (Table 1). NTX is in line structurally with TsTX-Kα up to residue 23 and comes back into structural frame at residue G26 of TsTX-Kα. While the insertion of this serine residue (S24) could cause major structural and functional differences between TsTX-Kα and NTX, insertions are often well tolerated, and sometimes have only minimal effects on biological activity (*46*, *47*). This is true especially when the insertion occurs in a loop or region of random coil, as is the case for S24 in NTX. Indeed, comparison of the three-dimensional structures of TsTX-Kα and NTX reveals a bulge in the loop between the α-helix and the second β-strand that accommodates the single amino acid residue insertion in NTX (Figure 4B). Nonetheless, it is still likely that this bulge may account for the 30-fold lower affinity that NTX has for voltage-gated squid channels (Table 4).

Model of the Interaction between TsTX-Kα and sqKv1A. To examine further specific interactions between sqKv1A and TsTX-Kα, the average NMR structure of TsTX-Kα was used to model the toxin bound to sqKv1A. As a first step, the toxin was manually docked in a homology model of sqKv1A (based on KscA). The preliminary model had very little observable van der Waals overlap, but was nevertheless subjected to energy minimization. The final energy-minimized structure successfully eliminated all van der Waals contacts, and retained ideal bond lengths, angles, and planarities. A minimal amount of structural perturbation of the toxin was necessary during energy minimization as judged by the small rmsd value between the manually docked structure and the final energy-minimized structure for backbone atoms of the toxin (0.71 Å).

While in general modeling based on homology should be interpreted cautiously (i.e., especially in regions of amino acid differences), the model illustrated in Figure 5 does satisfy the three experimental criteria used during the docking procedure. First, as found for AgTX2 bound to the KscA channel, K27 of TsTX-Kα is nearby (~3 Å) the backbone carbonyl oxygen atoms of Y371 at the mouth of the pore. The occlusion of the pore by K27 is a critical feature of this model and is supported by mutagenesis studies of TsTX-Kα (Figure 1) and by similar studies with several members of the α-K toxin family (*3*, *36*, *48*). Another critical residue identified in the *Shaker* family of channel−toxin interactions is M29 (*31*). Mutant cycle analysis with CTX and the *Shaker* channel indicate that M29 of CTX is nearby T449 (3−4.5 Å) of the channel (*31*). This is analogous to an interaction between M29 of TsTX-Kα and S375 of sqKv1A, which is satisfied in the TsTX-Kα−sqKv1A model (Table 5). Last, R8 does not approach H351 on any of the α-subunits of sqKv1A (>5 Å). This feature is consistent with the fact that mutagenesis of R8 (R8A) has very little effect on the pH dependence of toxin blocking (W. F. Gilly and M. Hayhurst, unpublished data). While not used as constraints, several other previously characterized α-K toxin−K^+ channel interactions (G9−S375, S10−D373, G31−H351, and P37−V377) were also satisfied in the TsTX-Kα−sqKv1A model (refs *31*, *32*, *41*, *42*, and *49* and Table 5).

DISCUSSION

The native squid K^+ channel expressed in the giant axon system, often termed the classical delayed rectifier channel, is thought to be composed of sqKv1A α-subunits. In preliminary experiments, we observed that TsTX-Kα blocks these noninactivating K^+ channels in squid giant axons and giant fiber lobe (GFL) (*12*). Additionally, this native channel displays pH-dependent blocking by TsTX-Kα. In this report, we show that TsTX-Kα blocks cloned sqKv1A channels expressed in oocytes (*8*) with a K_d of 10 nM (Figure 1), and that the blocking is also pH-dependent. These facts provide strong support for the idea that α-subunits of sqKv1A correspond to those existing in native channels (*8*). We have

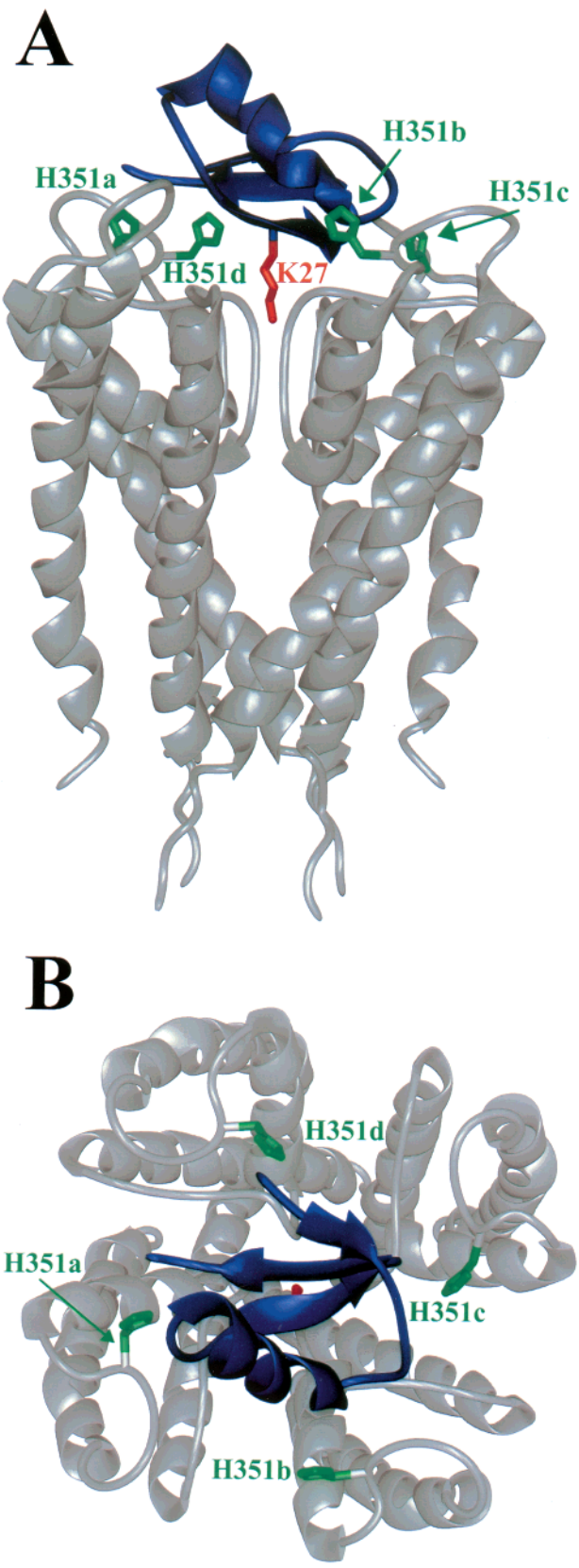

FIGURE 5: Homology model of TsTX-Kα docked to the sqKv1A channel. (A) The average NMR structure of TsTX-Kα (blue) is docked into a model of sqKv1A (gray). Shown in green are histidine residues (H351) from each α-subunit (arbitrarily labeled a−d), and in red is K27 from TsTX-Kα. (B) Top view of TsTX-Kα docked into a model for sqKv1A with the same color scheme used in panel A.

therefore used sqKv1A channels to further characterize the pH-dependent blocking by TsTX-Kα as observed for both native and cloned squid channels.

Chemical modification and site-directed mutagenesis indicate that a lone histidine residue on the sqKv1A α-subunit (H351) is responsible for the pH dependence observed in the high-affinity TsTX-Kα blocking (Figure 1). When His-351 is chemically modified by DEPC treatment or mutated to glycine (H351G), blocking by TsTX-Kα is unaffected by extracellular pH (Figure 1). Interestingly, position 351 of sqKv1A is analogous to position 425 in *Shaker* (Table 2). This well-characterized residue in *Shaker* is clearly involved in binding α-K toxins because mutation of Phe-425 to Gly increases the CTX affinity by ~2000-fold (*43*). Furthermore, this single F425G channel mutation provided the background for subsequent detailed studies of the toxin−*Shaker* interaction (*43*). Mutant cycle analyses (*32*, *50*) involving Phe-425 of *Shaker* showed that this position is near Gly-10 on AgTX2 or threonine residues (T8 and T9) on CTX (Table 5). In addition, if Phe-425 of *Shaker* is mutated to a histidine, as found in wild-type sqKv1A (Table 2), then the affinity of the CTX block for this channel increases by 10-fold, and pH sensitivity is introduced (*51*, *52*), much like that observed for the TsTX-Kα−sqKv1A interaction.

The pH-dependent blocking of K^+ channels by CTX is thought to be due to electrostatic repulsion between protonated histidine residues on mutant *Shaker* (F425H) at low pH and positively charged residues on the toxins (*51*). For the CTX−*Shaker* complex, three residues of the toxin (K11, R25, and K31) are proposed to interact with His-425 of the mutant *Shaker* channel; a fourth residue (K34) was also suggested to be close enough to His-425 to influence the toxin's binding (*51*). In this model, Lys-11, Arg-25, and Lys-31 of CTX form the corners of a triangle asymmetrically positioned around Lys-27 such that each of the positively charged residues of CTX lies very close to a F425H mutation on one of the four *Shaker* α-subunits (*51*). This "electrostatic repulsion" model is supported by mutagenesis of CTX (K11Q, K31Q, and the double mutant K11Q/K31Q) which substantially reduces the pH dependence of blocking (*51*). However, all of these mutations greatly decrease toxin affinity even at high pH (pH 8.0), and this effect would seem to complicate this interpretation (*51*). Although this model of CTX binding is attractive, it is somewhat surprising that strong interactions between Shaker F425 and lysine residues on CTX were not evident in previous mutant cycle analyses (*32*, *40*, *42*, *49*, *53*).

The pH-dependent blocking of sqKv1A by TsTX-Kα is likely to be different from that proposed for the CTX−*Shaker* complex. This is because three charged residues that constitute the postulated "active" triangle on CTX (K11, R25, and K31) are all replaced with smaller, uncharged residues in TsTX-Kα (P11, A25, and G31, respectively). In fact, there are no basic residues from TsTX-Kα positioned like K11, R25, or K31 of CTX when the three-dimensional structures of TsTX-Kα and CTX are compared (Figure 4A). Only one residue of TsTX-Kα, R8, is located in three-dimensional space remotely like one of the three positively charged residues of CTX (K11, R25, or K31), but it appears to protrude from the opposite surface of the toxin (Figure 4A). Moreover, mutation of this residue (R8A) has very little, if

Table 5: Comparison of Distances of Toxin−Channel Interactions Reported Previously to Those in the TsTX-Kα−sqKv1A Model

CTX residue	toxin	toxin residue	channel type	channel residue	reported distance	TsTX-Kα residue	sqKv1A residue	model distance	ref
8	CTX	T8/T9	*Shaker*	F425	<5 Å	R8	H351	5−6 Å[a]	*49*
9	AgTX2	G10	*Shaker*	F425	NR	G9	H351	7 Å	*32*
9	AgTX2	G10	*Shaker*	T449	NR	G9	S375	4 Å	*32*
10	AgTX2	S11	*Shaker*	D447	NR	S10	D373	4−6 Å	*32*
11	CTX	K11	*Shaker*	K427	∼5 Å	P11	K353	9 Å	*42*
14	CTX	W14	Kv1.3	G380	NR	L14	H351	8 Å	*41*
14	KTX	L15	Kv1.3	G380	NR	L14	H351	8 Å	*41*
24	AgTX2	R24	*Shaker*	D431	NR	A24	D357	14 Å[b]	*32*
24	AgTX2	R24	*Shaker*	D431	NR	A24	D357	14 Å[b]	*40*
25	CTX	R25	Kv1.3	H404	2.4−6 Å	A25	S375	9 Å[a,b]	*41*
25	CTX	R25	Kv1.3	D386	6−8 Å	A25	D357	10 Å[a,b]	*41*
25	KTX	R24	Kv1.3	H404	5.3−8.5 Å	A25	S375	9 Å[a,b]	*41*
25	KTX	R24	Kv1.3	D386	3−4 Å	A25	D357	10 Å[a,b]	*41*
25	AgTX2	F25	*Shaker*	M448	NR	A25	M374	8 Å[a,b]	*32*
26	KTX	F25	Kv1.3	H404	2.4−6 Å	G26	S375	8 Å[a,b]	*41*
27	AgTX2	K27	*Shaker*	Y445	NR	K27	Y371	3 Å	*32*
29	CTX	M29	*Shaker*	T449	3−4.5 Å	M29	S375	3 Å	*31*
31	AgTX2	R31	*Shaker*	K427	NR	G31	K353	8 Å[c]	*32*
31	AgTX2	R31	*Shaker*	A432	NR	G31	S358	13 Å[c]	*32*
31	AgTX2	R31	*Shaker*	D431	NR	G31	D357	11 Å[c]	*40*
31	CTX	K31	Kv1.3	G380	NR	G31	H351	5 Å[c]	*41*
31	KTX	R31	Kv1.3	G380	NR	G31	H351	5 Å[c]	*41*
37	AgTX2	P37	*Shaker*	V451	NR	P37	V377	4 Å	*32*

[a] These residues are very different in TsTX-Kα compared to CTX and are proposed to influence the selectivity of these toxins for sqKv1A channels. Therefore, a difference in their position in relation to the K^+ channel may be expected. See the text for a more detailed discussion. [b] Differences in the reported distance and that observed in the TsTX-Kα−sqKv1A model are likely due to differences in the length of the side chains. [c] Although this distance agrees with mutagenesis data, the difference in β-turn between CTX and TsTX-Kα (type I vs I′, respectively) places residue 31 of each toxin in very different positions (Figure 4A). For example, G31 of TsTX-Kα is close to H351/G380 on a subunit different from that observed for K31 of CTX.

any, effect on the pH-dependent blocking of sqKv1A by TsTX-Kα (Table 4 and unpublished data). Therefore, it is clear that TsTX-Kα must bind sqKv1A in a manner somewhat different from that found for CTX binding to *Shaker*.

The three-dimensional structure of TsTX-Kα and the model of the toxin−sqKv1A complex determined here were used to examine this toxin−channel interaction in more detail. The modeling of the channel was possible because the sequences of the pore and turret regions of sqKv1A (residues 347−379) are 84% homologous to those of *Shaker*, and most residues that differ are relatively conservative substitutions (Table 2). Also, on the basis of site-directed mutagenesis studies (Table 4), the role of K27 in K^+ channel blocking by TsTX-Kα is similar to that of other α-K toxins. As found in CTX, site-directed mutations of K27 in TsTX-Kα (i.e., K27A, K27R, and K27E) markedly reduced the channel blocking activity of the toxin (Table 4). These data are consistent with models of other α-K toxin−channel interactions (*4*, *34*, *37*, *48*, *51*) and the idea that K27 of TsTX-Kα inserts into the pore of sqKv1A and physically occludes the flow of potassium ions (Figure 5).

In the model of TsTX-Kα bound to sqKv1A (Figure 5), two lysine residues of TsTX-Kα are candidates for electrostatic repulsion with protonated H351 residues on sqKv1A, and this may be the reason there is a pH dependence of blocking by TsTX-Kα. In this complex, H351 residues of two opposite subunits of the channel (subunits a and c) are nearby (<2.8 Å) K6 and K23 of the toxin (Figure 6). All other basic residues of TsTX-Kα are either farther away or facing the solvent (i.e., on the toxin surface facing away from the channel mouth). For any of these more distant positively charged residues to interact with H351, the toxin would have to be reoriented in the channel in such a way that K27 could no longer occlude the ion selective pore. A second interaction that could affect TsTX-Kα binding involves P11 of the toxin. This proline residue is nearby H351 on another subunit (subunit b) of sqKv1A (∼3.5 Å) in the docking model (Figure 6), and it is possible that protonation of the histidine residue is sufficient to introduce steric overlap. Similarly, F2 of TsTX-Kα is close (∼3.5 Å) to H351 on subunit d of the channel such that steric interactions may disrupt toxin blocking of sqKv1A at acidic pH values (Figure 6). Thus, the pH dependence observed for the TsTX-Kα blocking of sqKv1A is most likely due to electrostatic repulsion between K6 and/or K23 of the toxin and protonated H351 of the channel, but P11 and/or F2 may also contribute somewhat to the decreased toxin binding activity observed at lower pH values.

CONCLUSIONS

Members of the α-K toxin family have subtle differences in side chain identity and position that can affect toxin−channel interactions (*3*). In this report, the high-affinity blocking of the cloned sqKv1A channel by TsTX-Kα was found to be pH-dependent. This pH dependence is due to a histidine residue (H351) in the outer vestibule of the channel, which likely repels positively charged residues on the toxin at low pH. As with other α-K toxin−channel interactions, K27 is a critical residue for the TsTX-Kα blocking of sqKv1A. However, a model for the sqKv1A−TsTX-Kα complex indicates that this toxin−channel interaction is somewhat different from that observed for other α-K toxins

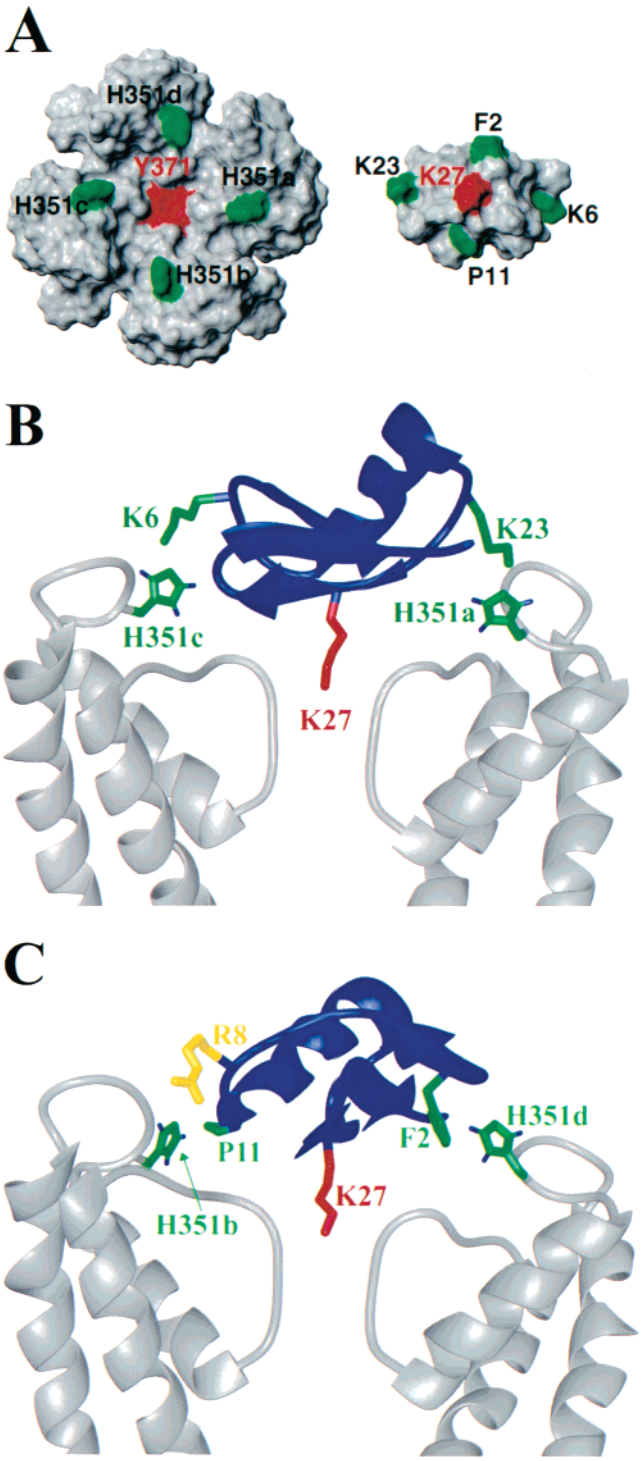

FIGURE 6: Views of the interaction between TsTX-Kα and sqKv1A. (A) Space-filling model of sqKv1A and TsTX-Kα illustrating the region on sqKv1A (red) that interacts with K27 of TsTX-Kα. Also shown is His-351 on each subunit (in green) of the 4-fold symmetric K^+ channel. Each of these histidine residues (H351; labeled a−d) could interact with residues on the toxin (F2, K6, P11, and K23; shown in green). These interactions could be responsible for the pH dependence of toxin binding. (B) Possible electrostatic repulsion between protonated H351 and positive residues on the toxin (K6 and K23; green) is illustrated. (C) View of the TsTX-Kα−sqKv1A complex illustrating a potential steric overlap between protonated H351 (green) and residues on the toxin (F2 and P11; green). Also shown is R8 of TsTX-Kα (yellow).

such as CTX or NTX despite the fact that K27 occludes the pore in all three toxin−channel complexes.

ACKNOWLEDGMENT

We acknowledge Dr. Donna M. Baldisseri for assistance with collection of the NMR spectra, Robert Rogowski for his assistance with purification of TsTX-Kα, and Dr. Lewis Pannell for identification of toxins (wild-type and mutants) by mass spectrometry. Molecular images were produced using the MidasPlus program from the Computer Graphics Laboratory, University of California, San Francisco (supported by NIH Grant RR-01081).

SUPPORTING INFORMATION AVAILABLE

Resonance assignments for TsTX-Kα, the amide region from the 200 ms NOESY spectrum of TsTX-Kα , a schematic diagram for the β-sheet region of TsTX-Kα, the sequence distribution of the NOE constraints used for structural calculations, and the Ramachandran plot of the lowest-energy structure. This material is available free of charge via the Internet at http://pubs.acs.org.

REFERENCES

1. Strong, P. N. (1990) *Pharmacol. Ther. 46*, 137−162.
2. Dreyer, F. (1990) *Rev. Physiol., Biochem. Pharmacol. 115*, 93−136.
3. Tenenholz, T. C., Klenk, K. C., Matteson, D. R., Blaustein, M. P., and Weber, D. J. (2000) *Rev. Physiol., Biochem. Pharmacol. 140*, 135−185.
4. Miller, C. (1995) *Neuron 15*, 5−10.
5. Grissmer, S., Nguyen, A. N., Aiyar, J., Hanson, D. C., Mather, R. J., Gutman, G. A., Karmilowicz, M. J., Auperin, D. D., and Chandy, K. G. (1994) *Mol. Pharmacol. 45*, 1227−12234.
6. Stuhmer, W., Ruppersberg, J. P., Schroter, K. H., Sakmann, B., Stocker, M., Giese, K. P., Perschke, A., Baumann, A., and Pongs, O. (1989) *EMBO J. 8*, 3235−3244.
7. Mathes, C., Rosenthal, J. J., Armstrong, G. M., and Gilly, W. F. (1997) *J. Gen. Physiol. 109*, 435−448.
8. Rosenthal, J. J., Vickery, R. G., and Gilly, W. F. (1996) *J. Gen. Physiol. 108*, 207−219.
9. Rosenthal, J. J., Liu, T. I., and Gilly, W. F. (1997) *J. Neurosci. 17*, 5070−5079.
10. Nealey, T., Spires, S., Eatock, R. A., and Begenisich, T. (1993) *J. Membr. Biol. 132*, 13−25.
11. Perozo, E., Jong, D. S., and Bezanilla, F. (1991) *J. Gen. Physiol. 98*, 19−34.
12. Dudlak, C. S., Jerng, H. H., and Gilly, W. F. (2000) *Biophys. J. 78*, 571.
13. Klenk, K. C., Tenenholz, T. C., Rogowski, R. S., Blaustein, M. P., and Weber, D. J. (1998) *Biophys. J. 76*, A326.
14. Klenk, K. C., Tenenholz, T. C., Blaustein, M. P., and Weber, D. J. (2000) *Proteins: Struct., Funct., Genet. 38*, 441−449.
15. Tenenholz, T. C., Rogowski, R. S., Collins, J. H., Blaustein, M. P., and Weber, D. J. (1997) *Biochemistry 36*, 2763−2771.
16. Blaustein, M. P., Rogowski, R. S., Schneider, M. J., and Krueger, B. K. (1991) *Mol. Pharmacol. 40*, 932−942.
17. Bartschat, D. K., and Blaustein, M. P. (1985) *J. Physiol. 361*, 419−440.
18. Howell, M. L., and Blumenthal, K. M. (1989) *J. Biol. Chem. 264*, 15268−15273.
19. Liu, T. I., Lebaric, Z. N., Rosenthal, J. J., and Gilly, W. F. (2001) *J. Neurophysiol.* (in press).
20. McFarlane, M. B., and Gilly, W. F. (1996) *Proc. Natl. Acad. Sci. U.S.A. 93*, 5067−5071.
21. Spires, S., and Begenisich, T. (1990) *J. Gen. Physiol. 96*, 757−775.
22. Piotto, M., Saudek, V., and Sklenar, V. (1992) *J. Biomol. NMR 2*, 661−665.
23. Delaglio, F., Grzesiek, S., Vuister, G. W., Zhu, G., Pfeifer, J., and Bax, A. (1995) *J. Biomol. NMR 6*, 277−293.
24. Wüthrich, K. (1986) *NMR of Proteins and Nucleic Acids*, John Wiley, New York.

25. Bax, A., and Davis, D. G. (1985) *J. Magn. Reson. 65*, 355−360.
26. Macura, S., and Ernst, R. R. (1980) *Mol. Phys. 41*, 95−117.
27. Griesinger, C., and Ernst, R. R. (1987) *J. Magn. Reson. 75*, 261.
28. Griesinger, C., Sørensen, O. W., and Ernst, R. R. (1987) *J. Magn. Reson. 75*, 474−492.
29. Brünger, A. T. (1992) *XPLOR*, version 3.1, Yale University Press, New Haven, CT.
30. Doyle, D. A., Cabral, J. M., Pfuetzner, R. A., Kuo, A., Gulbis, J. M., Cohen, S. L., Chait, B. T., and MacKinnon, R. (1998) *Science 280*, 69−77.
31. Naranjo, D., and Miller, C. (1996) *Neuron 16*, 123−130.
32. Ranganathan, R., Lewis, J. H., and MacKinnon, R. (1996) *Neuron 16*, 131−139.
33. Brooks, B. R., Bruccoleri, R. E., Olafson, B. D., States, D. J., Swaminathan, S., and Karplus, M. (1983) *J. Comput. Chem. 4*, 187−217.
34. MacKinnon, R., and Miller, C. (1988) *J. Gen. Physiol. 91*, 335−349.
35. Stampe, P., Kolmakova-Partensky, L., and Miller, C. (1994) *Biochemistry 33*, 443−450.
36. Park, C. S., and Miller, C. (1992) *Neuron 9*, 307−313.
37. Park, C. S., and Miller, C. (1992) *Biochemistry 31*, 7749−7755.
38. Wishart, D. S., Sykes, B. D., and Richards, F. M. (1992) *Biochemistry 31*, 1647−1651.
39. Harper, E. T., and Rose, G. D. (1993) *Biochemistry 32*, 7605−7609.
40. Hidalgo, P., and MacKinnon, R. (1995) *Science 268*, 307−310.
41. Aiyar, J., Withka, J. M., Rizzi, J. P., Singleton, D. H., Andrews, G. C., Lin, W., Boyd, J., Hanson, D. C., Simon, M., Dethlefs, B., et al. (1995) *Neuron 15*, 1169−1181.
42. Stocker, M., and Miller, C. (1994) *Proc. Natl. Acad. Sci. U.S.A. 91*, 9509−9513.
43. Goldstein, S. A., and Miller, C. (1992) *Biophys. J. 62*, 5−7.
44. Bontems, F., Roumestand, C., Boyot, P., Gilquin, B., Doljansky, Y., Menez, A., and Toma, F. (1991) *Eur. J. Biochem. 196*, 19−28.
45. Carbone, E., Wanke, E., Prestipino, G., Possani, L. D., and Maelicke, A. (1982) *Nature 296*, 90−91.
46. Shortle, D., and Sondek, J. (1995) *Curr. Opin. Biotechnol. 6*, 387−393.
47. Sondek, J., and Shortle, D. (1990) *Proteins 7*, 299−305.
48. MacKinnon, R., Cohen, S. L., Kuo, A., Lee, A., and Chait, B. T. (1998) *Science 280*, 106−109.
49. Goldstein, S. A., Pheasant, D. J., and Miller, C. (1994) *Neuron 12*, 1377−1388.
50. Gross, A., and MacKinnon, R. (1996) *Neuron 16*, 399−406.
51. Thompson, J., and Begenisich, T. (2000) *Biophys. J. 78*, 2382−2391.
52. Perez-Cornejo, P., Stampe, P., and Begenisich, T. (1998) *J. Gen. Physiol. 111*, 441−450.
53. Aiyar, J., Rizzi, J. P., Gutman, G. A., and Chandy, K. G. (1996) *J. Biol. Chem. 271*, 31013−31016.
54. Tytgat, J., Chandy, K. G., Garcia, M. L., Gutman, G. A., Martin-Eauclaire, M.-F., van der Walt, J. J., and Possani, L. D. (1999) *Trends Pharmacol. Sci. 20*, 444−447.
55. Jan, L. Y., and Jan, Y. N. (1997) *Annu. Rev. Neurosci. 20*, 91−123.
56. Laskowski, R. A., MacArthur, M. W., Moss, D. S., and Thornton, J. M. (1993) *J. Appl. Crystallogr. 26*, 283−291.

BI010173G